

The drifting subpulses of PSR B0031–07 and its synchronously modulated radio polarization

C.D. Ilie¹, P. Weltevrede^{1*}, S. Johnston² and T. Chen¹

¹University of Manchester, Jodrell Bank Centre of Astrophysics, Alan Turing Building, Manchester, M13 9PL, United Kingdom

²CSIRO Astronomy and Space Science, Australia Telescope National Facility, PO Box 76, Epping, NSW 1710, Australia

Accepted XXX. Received YYY; in original form ZZZ

ABSTRACT

We establish that for PSR B0031–07 the orthogonal polarization modes switch at a single pulse level synchronously with the periodic drifting subpulses seen in total intensity. There are only four other pulsars known for which this phenomenon is observed. PSR B0031–07 is unique as it is the only source in this group which has multiple stable drift modes. For both drift modes visible at our observing frequency centered at 1369 MHz, the modulation of polarization modes is synchronous with the drifting subpulses. In one of the drift modes, a discontinuity in the modulation pattern of polarization properties occurs halfway through the pulse, coinciding with a slight change in the slope of the intensity drift band. In contrast to what has been suggested for this pulsar in the past, this, plus other differences in the polarization of the modulated emission observed for the two drift modes, suggests that a drift mode change is more than a change in the underlying carousel radius and that magnetospheric propagation effects play an important role. The ellipticity evolves asymmetrically in time during the modulation cycle, which in the framework of a carousel model implies that the polarized sub-beams are asymmetric with respect to the sense of circulation, something which is not observed for other pulsars. Birefringence in the magnetosphere, resulting in the orthogonal polarization modes to spatially separate, is not enough to explain these results. It is argued that more complex magnetospheric processes, which possibly allow conversion between orthogonal polarization modes, play a role.

Key words: pulsars: general, polarization, pulsars:individual: PSR B0031–07

1 INTRODUCTION

Significant progress has been made in understanding the mechanism responsible for the observed coherent radio emission of pulsars since their discovery more than 50 years ago (Hewish et al. 1968). Nevertheless, due to the complexity of the observed emission of pulsars, there is not yet a theoretical model which is able to account for all the diverse phenomenology. The work presented in this paper aims to examine the connection between the organised intensity variability seen in single pulses and the synchronous periodic switching of the polarization properties, in particular the position angle (PA), between two orthogonal polarization states. Implications for the radio emission mechanism are discussed.

Although the individual pulses of pulsars are known to show chaotic changes in shape, many show systematic variations such that the emission is observed to shift in rotational

phase in an organised manner, producing structures in the form of oblique intensity bands in the pulse-stack. This is illustrated in Fig. 1 for PSR B0031–07 (J0034–0721). This phenomenon is referred to as *drifting subpulses* and was first seen in pulsars by Drake & Craft (1968). The pattern can be defined with two periodicities: P_2 , the spacing between two consecutive subpulses in rotational phase (or pulse longitude) and P_3 , the separation between the diagonal drift bands in pulse number (or pulse periods P). Several authors (Weltevrede et al. 2006, 2007; Basu et al. 2016, 2019) have investigated the organised variability of single pulses and concluded that subpulse drifting is common in pulsars, being detectable in about half the pulsars investigated. Hence, the phenomenon is thought to be an essential component of the radio emission mechanism.

The most well established model to explain drifting subpulses is known as the *carousel model* (Ruderman & Sutherland 1975). In this model, the emission beam consists of smaller sub-beams which rotate around the magnetic axis due to an $\vec{E} \times \vec{B}$ drift force. Individual subpulses corre-

* email: patrick.weltevrede@manchester.ac.uk

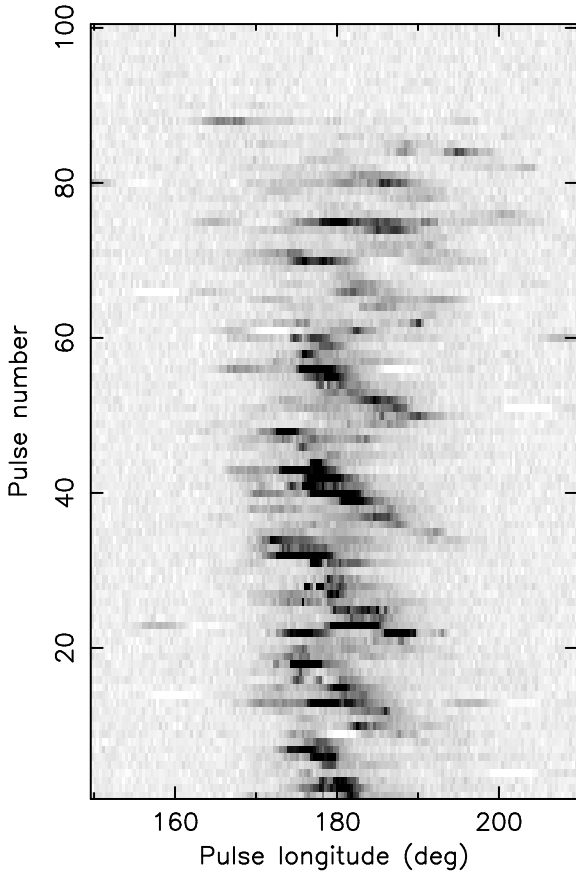


Figure 1. A small interval of 100 pulses of PSR B0031–07 halfway through the first observation at a centre frequency of 1369 MHz. Drift mode A drift bands (up to pulse number 60) are followed by mode B drift bands and a null. In this figure the brightest features are saturated (the colour range covers $\sim 20\%$ of the dynamic range) to reveal weaker emission.

spond to these sub-beams and because of the motion of the carousel, each sub-beam progressively moves across the line of sight of an observer, resulting in the systematic shift as a function of pulse longitude. Since Ruderman & Sutherland (1975), many authors have either refined the carousel model (e.g. Deshpande & Rankin 1999; Gil & Sendyk 2003; Wright 2003; van Leeuwen & Timokhin 2012; Hassall et al. 2013) or suggested alternative models which could explain drifting subpulses (e.g. Clemens & Rosen 2004; Gogoberidze et al. 2005; Fung et al. 2006).

The PA of some pulsars trace an S-shaped swing during a stellar rotation. This is explained by the Rotating Vector Model (RVM) (Radhakrishnan & Cooke 1969; Komesaroff 1970) as the change in projection of the dipolar magnetic field lines on the plane of the sky. In a number of pulsars, the gradual S-shape is interrupted by discontinuities in the shape of 90° jumps in the PA. These are explained with the co-existence of two Orthogonally Polarized Modes (OPMs) of radiation (Manchester et al. 1975; Backer et al. 1976). The origin of these OPMs, and the reason why different OPMs can dominate in different parts of a pulse profile, are still uncertain. Some authors (e.g. Gangadhara 1997) suggested that the production of OPMs is intrinsic to the radio emission mechanism. Other authors (e.g. Melrose 1979; Allen &

Melrose 1982; Arons & Barnard 1986) suggested that the two OPMs are the two natural modes of propagation in the highly-relativistic magnetized plasma inside the pulsar magnetosphere. These two propagation modes are the Ordinary mode (O mode) and the eXtraordinary mode (X mode), which are predicted to be linearly polarized and orthogonal to each other.

For four pulsars it is observed that the dominant OPM periodically switches, and that this occurs synchronous with the drifting subpulses as observed in total intensity. Ramachandran et al. (2002) observed sharp 90° OPM transitions in the subpulses of PSR B0809+74, which explained the periodic deviations from the RVM which were reported by Taylor et al. (1971) for that pulsar. Ramachandran et al. (2002) showed that the flips between the dominant OPMs occur synchronous with the drifting subpulses. This finding was soon followed by the discovery of similar behaviour in PSR B1237+25 (Rankin & Ramachandran 2003), and in PSRs B0320+39 and B0818–13 (Edwards 2004). For PSR B1237+25 the strict synchrony of the OPM flips and the drifting subpulses is not established, since no technique such as P_3 -folding (see Sect. 3.4) was used,

In order to explain the fact that, for some pulsars, the switches between OPMs are modulated by the periodicity of drifting subpulses, the carousel model needed some revision. Rankin & Ramachandran (2003) suggested that a single circulating carousel system (i.e. the pattern of discharges in the polar gap) produces two “images” of emission, each correspond to one of the observed OPMs. An azimuthal offset between the two images (with respect to the magnetic axis) would result in the observed periodic flips in the dominant PA. The two images are believed to arise due to birefringence in the pulsar magnetosphere (Rankin et al. 2006). This is expected since the X mode is not affected by refraction, thus it propagates in a straight path from the emitting region, while the O mode experiences refraction and therefore propagates on a curved path before escaping the pulsar magnetosphere (e.g. Petrova & Lyubarskii 2000; Petrova 2001; Lyubarsky 2002; Weltevrede et al. 2003). Hence, two images of the carousel will be produced; each image has mutually orthogonal polarization and could be magnified differently.

In this work, we show that modulation of OPMs synchronous with the drifting subpulses exists for PSR B0031–07. This is a particularly interesting and widely studied pulsar, as it displays drifting subpulses with three different stable drift modes. These are modes A ($P_3 \simeq 13P$), B ($P_3 \simeq 7P$) and C ($P_3 \simeq 4P$) (Huguenin et al. 1970), where P_3 is found to be variable within a given mode as well (McSweeney et al. 2017). The detectability of these modes depends on the observing frequency (e.g. Smits et al. 2005, 2007). For example, at 1.4 GHz only modes A and B have been observed (Smits et al. 2007). Manchester (1975) investigated the polarization properties of this pulsar and reported the presence of two OPMs. Our investigation builds on an initial analysis presented in a Masters thesis by Chen (2015) and preliminary results were published in Ilie & Weltevrede (2018). However, detailed analysis was hindered by instrumental variations on timescales comparable with the pulsar period P . In this analysis, we describe the observed behaviour in more detail using new data and discuss potential interpretations.

The structure of this paper is as follows. Sect. 2 de-

scribes the observations of PSR B0031–07. In Sect. 3.1, it is explained how the data is separated in multiple drift modes and fluctuation analysis is used (Sect. 3.2) to confirm that this is done successfully. The polarization properties of this pulsar are discussed in depth in Sect. 3.3 before in Sect. 3.4 it is established that the observed OPMs switch synchronously with the drifting subpulses. The results are discussed in Sect. 4 and the conclusions are presented in Sect. 5.

2 OBSERVATIONS

Two observations of PSR B0031–07 are described in this paper, which were performed using the H-OH receiver of the Parkes telescope with a bandwidth of 256 MHz, split into 512 frequency channels, centred at 1369 MHz. The data was recorded with the backend system known as the Parkes Digital FilterBank PDFB4. The first observation was made on 2016 April 9 and the second on 2016 August 29. In the two observations 13,622 and 7,951 individual pulses were recorded respectively.

Data was de-dispersed, de-Faraday rotated and folded off-line using DSPSR (van Straten & Bailes 2011) which allows the data to be re-organised in the form of a pulse-stack. After folding, the time resolution was 1024 pulse longitude bins per stellar rotation. The individual frequency channels were averaged, excluding those affected strongest by radio frequency interference (RFI). Some broad-band RFI was present in the data, including periodic bursts of RFI believed to be associated with a pump. Given the large number of pulses recorded, the effect on the analysis was found to be minimal. At the start of each observing session, a pulsed calibration signal was recorded for two minutes, while the telescope was pointed offset from the pulsar. This allows correction for differential gain and phase, which was applied to the data using the PSRCHIVE¹ software package.

The two observations were combined to improve the sensitivity. The rotational-phase alignment was achieved using a rotational ephemeris which was optimised for the rotation period P and its time derivative \dot{P} based on observations from the 76 m Lovell radio telescope in Jodrell Bank. Although the analysis presented in this paper is based on the combined observation, it was checked that the results are consistent with those obtained from the two individual observations.

3 ANALYSIS

All analysis in this section was performed with PSRSALSA² (Weltevrede 2016).

3.1 Drift mode identification

A small interval of the pulse-stack of PSR B0031–07 containing 100 consecutive pulses is displayed in Fig. 1, showing several mode A drift bands up to pulse number 60. After this, shallower mode B drift bands can be seen followed by a null

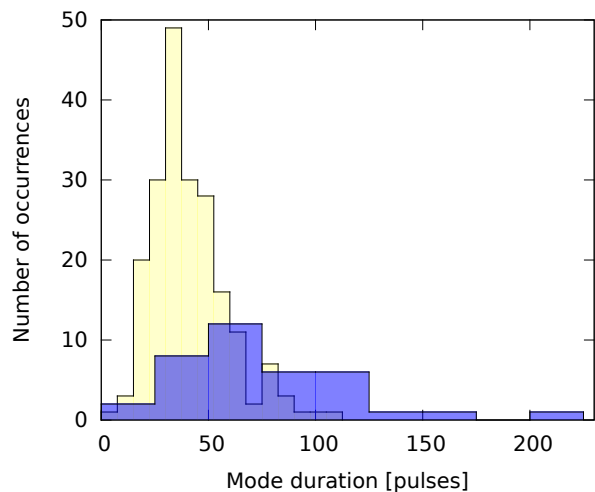


Figure 2. Distributions of the duration of stretches of data in a certain drift mode. Drift modes A and B correspond to the light and dark colored distribution respectively (yellow and blue in the online version).

state, during which the radio emission mechanism appears to be inactive. As noted by for example Smits et al. (2005), the pattern of drifting subpulses is clearer at lower observing frequencies. Nevertheless, the choice was made to observe at this frequency because of the excellent performance of the Parkes telescope in producing polarization calibrated pulsar data (see e.g. Weltevrede & Johnston 2008; Johnston & Kerr 2018).

As we are interested in the modulation of the OPMs, the analysis which follows requires the data to be separated in the different drift modes, since each drift mode has different polarization and modulation properties. The adopted methodology of mode separation is as follows. The pulse-stack was visually inspected. One occurrence of mode C was seen in the pulse-stack (the length of the whole observation is ~ 5 hours), as several drift bands following an occurrence of mode B. However, due to the rarity of mode C, we did not attempt to include this mode in any further analysis. Each individual pulse was assigned one of the following categories: mode A, mode B, mode C, null state, or the emission was too weak to be classified. The last category was included in order to avoid possible mis-labeling weak emission. There were no individual pulses where RFI affected the mode identification.

Out of a total of 21,573 individual pulses, the pulsar was in a null state for 8,606 pulses (39.9%) and the pulsar was on (in one of the three drift states) for 43.1% of the time (9,294 pulses). For the rest of the pulses, emission was observed, but too weak to be classified reliably (17.0%). During the time the pulsar was on and classifiable, 30.5% of the time it was in mode A (2,838 pulses), 69.2% of the time it was in mode B (6,430 pulses) and 0.3% of the time it was in mode C (26 pulses). At 328 MHz, Smits et al. (2005) reported that PSR B0031–07 was on (in one of the three drift modes) 61.8% of the time (of which 17.8% mode A, 80.1% mode B and 2.1% mode C). This confirms that mode A is more common at higher radio frequencies (Smits et al. 2005, 2007). The null fraction as reported by Smits et al. (2005) is very similar.

¹ <http://psrchive.sourceforge.net/>

² <https://github.com/weltevrede/psrsalsa>

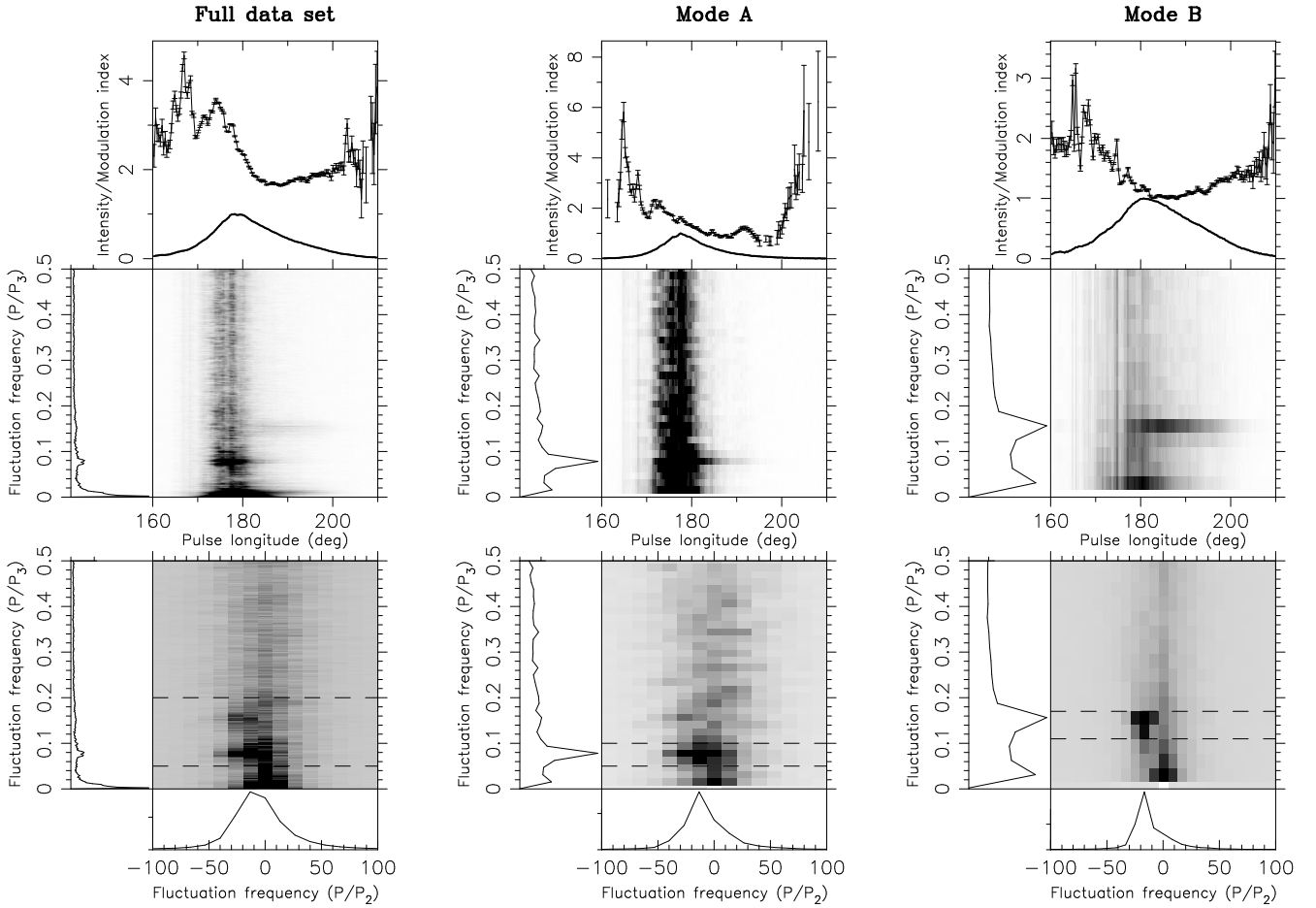


Figure 3. The results of a fluctuation analysis of PSR B0031–07. The top panels show the integrated pulse profiles, as well as the modulation index (data points with their associated uncertainties if its significance exceeds 3σ). The middle panel displays the LRFs with the horizontally integrated power shown in the side panel. The bottom panels show the 2DFS, with two side panels, which display the horizontally and (between the two dashed lines) vertically integrated power respectively. The brightest features in the grey-scale plots are saturated to highlight the weaker features. *Left:* The not-mode-separated data. *Middle:* Drift mode A. *Right:* Drift mode B.

Distributions of the duration of individual stretches of mode A and B data are shown in Fig. 2. From these plots, it can be seen that bursts of mode A emission tends to last longer compared to mode B emission. The mode A bursts last between ~ 25 and ~ 200 pulses (between 2 and 15 consecutive drift bands). Mode B bursts range from a few pulses up to 100 pulses (between 1 and 15 consecutive drift bands).

Mode separation is somewhat subjective because of variability in the emission unrelated to drifting subpulses. Nevertheless, a fluctuation analysis on the mode-separated data confirms that the mode separation was successful. The results of the fluctuation analysis on the total intensity both before and after mode separation are shown in Fig. 3. A detailed description of this figure is provided in the following subsections.

3.2 Fluctuation analysis

All fluctuation analysis described in this subsection was done in the spectral domain. See Weltevrede et al. 2006, 2007 for details about the methodology.

The modulation index quantifies how much the inten-

sity varies from pulse to pulse for a certain pulse longitude and is equal to the standard deviation of the intensity divided by its average. The modulation index, along with the pulse profile, is shown in the top panels of Fig. 3. This reveals an asymmetry such that the leading part of the profile is more strongly modulated, and that the two drift modes have different modulation properties. To quantify the periodicities in the data, and their difference for the two modes, fluctuation spectra are calculated.

The computation of the Longitude Resolved Fluctuation Spectrum (LRFs; Backer 1970) allows the investigation of the repetition frequency of the drifting subpulse pattern P_3 . The LRFs is obtained by averaging the power spectra obtained from blocks of pulses. For the not-mode-separated data large blocks of 512 pulses were used, which gives a high spectral resolution. For the mode-separated data, the choice of block size was made based on the typical mode length as inferred from Fig. 2. Since the pulses in each block must be continuous, a large block size implies limited data can be analysed. The mode A and B separated data was organised into sequences of 64 and 32 consecutive pulses respectively. Care was taken to only consider blocks in which all pulses

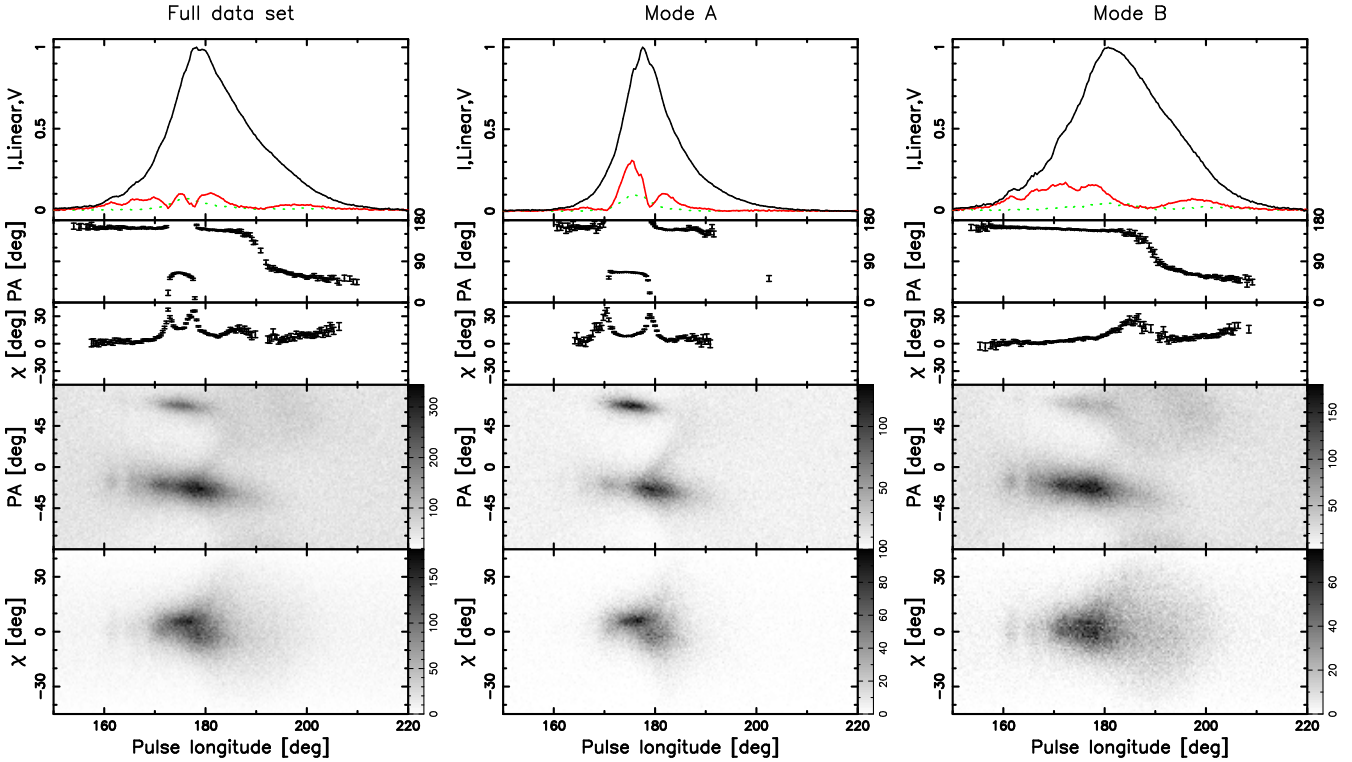


Figure 4. Polarization properties of PSR B0031–07. In the top panels, the total intensity pulse profile (black curve), linear polarization (red curve in the online version), and circular polarization (dotted curve which is green in the online version) are shown. The time averaged PA and ellipticity angle χ are shown in the second and third row of panels respectively. The bottom two rows of panels display the PA and χ distribution obtained for individual pulses when the significance of respectively L and $\sqrt{Q^2 + U^2 + V^2}$ exceeded 1σ (the required significance for the average PA and χ was 2σ). Note that the average PA swing is mapped between 0° and 180° , while the PA distribution covers -90° to 90° . *Top:* The not-mode-separated data. *Bottom left:* Mode A data. *Bottom right:* Mode B data.

were classified to be in the same mode and incomplete blocks were discarded from the analysis.

The LRFS for modes A and B and the non-mode-separated data are shown below the pulse profiles in Fig. 3. The left-most LRFS in Fig. 3, which is based on the not-mode-separated data, reveals three main features. The first is centred at zero fluctuation frequency, pointing towards fluctuations with long timescales, and is likely to be associated to nulling and drift mode changes. There is a strong feature at a fluctuation frequency $P/P_3 \simeq 0.07$ cycles per period (cpp), indicating $P_3 \simeq P/0.07 \simeq 14P$ which corresponds to drift mode A. The fact that the feature is resolved in fluctuation frequency indicates that P_3 is variable. A weaker feature corresponding to mode B, which is more pronounced in the trailing half of the profile, can be seen at ~ 0.16 cpp or at $P_3 \simeq 6P$.

As a confirmation for the successful mode separation, in analysis of the mode-separated data (middle and right column in Fig. 3), only the periodicity of the drift mode of interest remains. This is most pronounced in the side panels, which show the horizontally integrated power.

To measure P_2 , or demonstrate the existence of drifting subpulses, the 2-Dimensional Fluctuation Spectrum (2DFS, Edwards & Stappers 2002) can be used. In the 2DFS (bottom row of panels in Fig. 3) there is power at the same P/P_3 frequencies as observed in the LRFS. The fact that the power is offset horizontally from zero, resulting in a neg-

ative P_2 , means that, as expected, the subpulses drift to the leading side of the profile (see Fig. 1 as well). P_3 and P_2 were measured for the mode-separated data by calculating the centroid of power in the 2DFS (taking care to account for systematic uncertainties, see Weltevrede et al. 2006). For mode A, this results in $P_3 = (13.0 \pm 0.2)P$ and $P_2 = (30^{+15}_{-10})^\circ$. For mode B, $P_3 = (6.9 \pm 0.2)P$ and $P_2 = (20^{+7}_{-5})^\circ$. These values are consistent with Fig. 1 and measurements by Smits et al. (2007) at 1167 MHz, as well as P_3 measurements by Huguenin et al. (1970) and Smits et al. (2005). The measurements are consistent with P_2 being identical for the different drift modes, as was noted by Huguenin et al. (1970).

3.3 Polarization properties

Looking at the top panels of Fig. 4, it is clear that modes A and B have significantly different intensity profiles and average polarization properties. The intensity profile of mode B peaks $\sim 5^\circ$ later in pulse longitude and the widths are also different. The measured 10%-widths of mode A and B are 28° and 44° respectively with a nominal error of 1° . This shift in peak location of the pulse profile, and the variation in width, have been observed at other frequencies as well (e.g. Vivekanand & Joshi 1997; Wright & Fowler 1981; Vivekanand & Joshi 1997; Smits et al. 2007).

The average linear polarization $L = \sqrt{Q^2 + U^2}$ and cir-

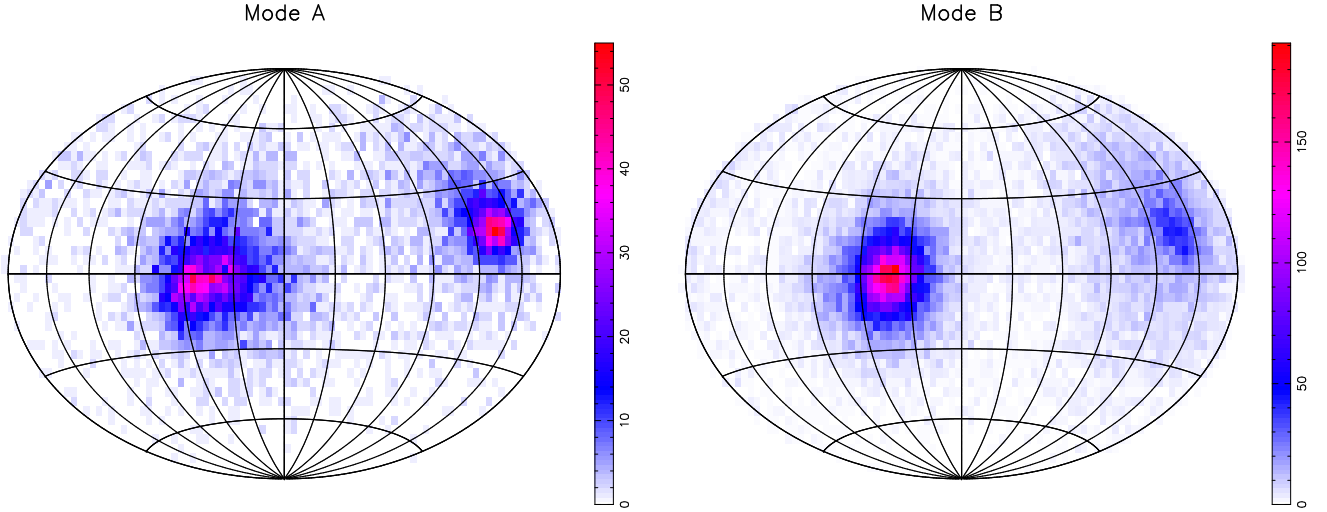


Figure 5. Distribution of polarization orientations on a Poincaré sphere projected using the Hammer equal area projection. Only emission with both L and total polarization exceeded a significance 1σ were included, and samples from all pulse longitudes in the pulse window were considered, after re-binning the data to 64 longitude bins per rotation. The effect of the PA-swing was compensated for to reduce smearing (see text). The latitudes represent great circles of constant χ separated by 30° with pure linear polarization being the equator. The north and south poles correspond pure circular polarization with a positive and negative Stokes V respectively. The meridians represent lines of constant PA, ranging from -90° (left) to 90° (right), in steps of 15° . *Left:* Mode A data. *Right:* Mode B data.

cular polarization V of the not-mode-separated data are low (where Q , U and V are Stokes parameters), as seen in the top panels of Fig. 4. In comparison, L in the mode-separated data is stronger, which suggests that different OPMs dominate for different drift modes, thereby causing depolarization when summed. The PA swings of the two drift modes are indeed different (see second row panels of Fig. 4). The two OPM jumps observed in the PA swing of the more strongly polarized mode A do not occur for mode B. The occurrence of OPM jumps in PSR B0031–07 is known to be frequency dependent (Smits et al. 2007). The ellipticity angle χ , defined via $\tan(2\chi) = V/L$, appears to peak where the two OPM transitions occur for mode A (see third row of panels of Fig. 4). For mode B, the ellipticity angle is small, except around longitude $\sim 189^\circ$ and towards the trailing edge of the profile.

To further investigate the existence of OPMs, the PA distribution of individual pulses was determined. The obtained distributions (see fourth row of panels in Fig. 4) reveal that at most pulse longitudes there is a mixture of OPMs observed for both modes A and B. We define the OPM observed at $\text{PA} \simeq 65^\circ$ as OPM_A , and the OPM at $\text{PA} \simeq -25^\circ$ as OPM_B . For drift mode B, OPM_B dominates up to pulse longitude $\sim 190^\circ$. Compared to drift mode B, OPM_A dominates much more frequently in the individual pulses of drift mode A. This is especially true between pulse longitudes $\sim 170^\circ$ and $\sim 180^\circ$, thereby explaining the jumps in the integrated PA swing. Since there is a mixture of OPMs, depolarization of the integrated profile can be expected, as is observed.

In the PA distribution of drift mode A (fourth panel in the middle column of Fig. 4), a structure can be seen flaring off upwards from OPM_B , starting at pulse longitude 178° and connecting with the other OPM at longitude $\sim 190^\circ$. Clearly the polarization state of the radiation is more

complex than an incoherent summation of two OPMs. This structure is only visible in the drift mode A data.

Unlike the drift mode B data, the mode A data has an ellipticity angle distribution (bottom row of panels in Fig. 4) which does appear to be bi-modal, with one component being significantly more linear than the other. The origin of the bi-modality is revealed by exploring the distribution of polarization orientations which can be visualised in the form of a Poincaré sphere (Fig. 5). The data was first re-binned into 64 pulse longitude bins, in order to increase the significance of each sample. Since the peaks in the PA distributions in Fig. 4 shift only slightly in PA as function of pulse longitude, especially where the polarized emission is strongest, the introduced depolarization because of rebinning is minimal. Nevertheless, to compensate for this effect, the Stokes Q and U parameters for each sample were rotated before rebinning such that the time-averaged PA-swing was removed from the data. This was done for each drift-mode separated dataset separately. After rebinning, the time-averaged PA-swing as measured from the re-binned data was re-introduced before producing the Poincaré spheres as shown in Fig. 5. The two OPMs manifest themselves as two islands offset by $\sim 180^\circ$ in longitude in the Poincaré sphere. OPM_A is clearly elliptical (appearing at the right hand side), while OPM_B is almost entirely linearly polarized.

The shown Poincaré spheres demonstrate that the two OPMs have polarization properties which are essentially independent on drift mode. OPM_A is clearly elliptical with $\chi \simeq 8^\circ$, while OPM_B is practically linear. This means that the two polarization modes are not situated on antipodal points on the Poincaré sphere. According to most theories, OPMs are expected to be orthogonal in both PA and ellipticity (e.g. Melrose et al. 2006), however deviations from orthogonality have been previously observed for other pulsars too (e.g. Edwards et al. 2003; Edwards 2004).

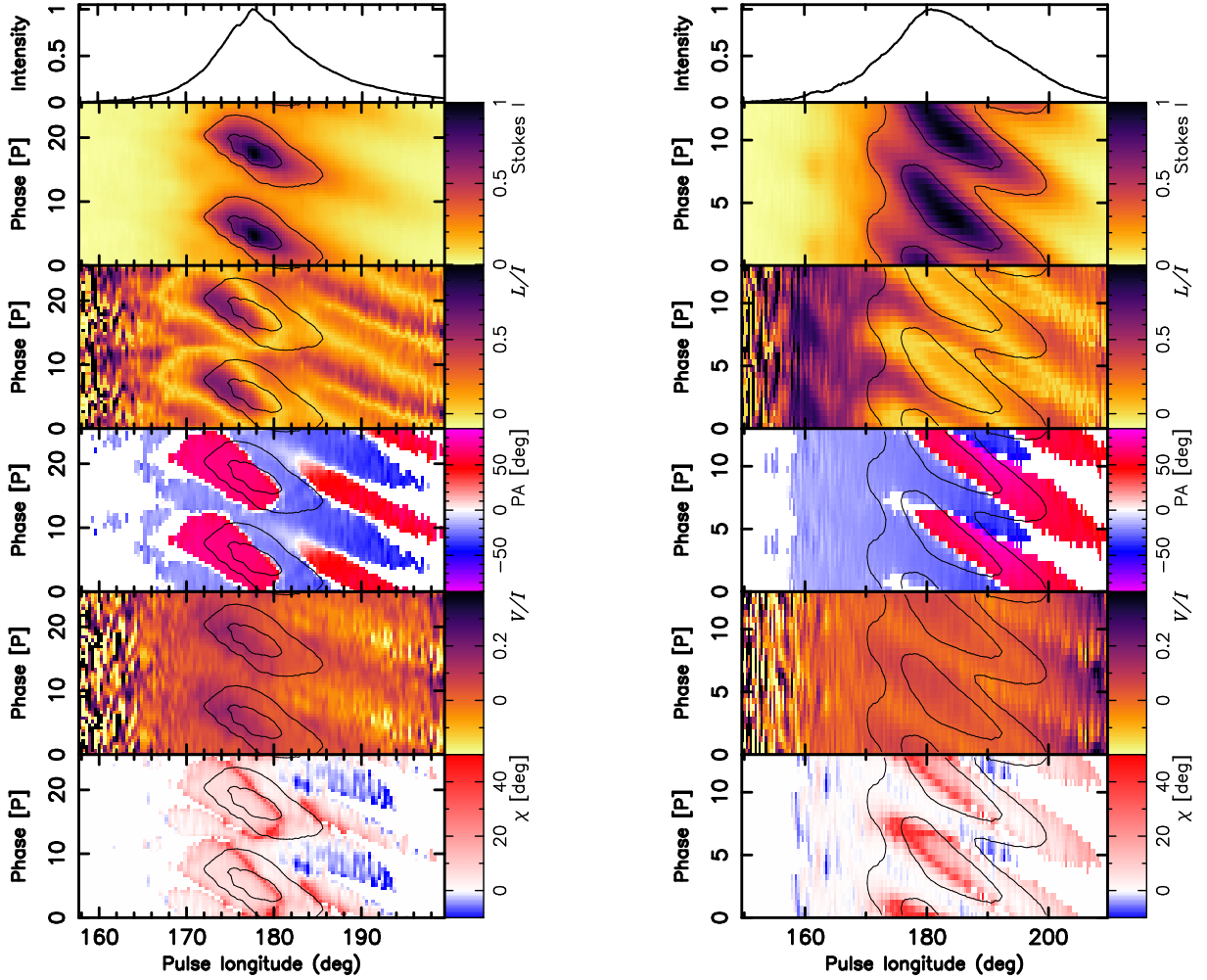


Figure 6. P_3 -folds of drift mode A (left) and B (right) for PSR B0031–07 are shown below the pulse profile. From top to bottom the P_3 -folds correspond to Stokes I , L/I , PA, V/I and χ . The modulation cycle is shown twice for continuity. The contours, which are identical in each panel, correspond to the drift band shape observed in Stokes I . The PA and χ are shown if the significance of respectively L and $\sqrt{Q^2 + U^2 + V^2}$ exceeds 3σ .

3.4 Periodic polarization variability

As is also explained in [Ilie & Weltevrede \(2018\)](#), P_3 -folding can reveal the relation between the two OPMs and the periodicity of drifting subpulses. P_3 -folding is the process where data is averaged over the modulation cycle which results in the average shape and properties of a drift band. Since P_3 is not fixed, but varies, as demonstrated in Sect. 3.2, these variations need to be taken into account when averaging successive drift bands over large stretches of data (e.g. [Deshpande & Rankin 2001](#); [van Leeuwen et al. 2002](#)). Here the variability was compensated for using a tool from the PSRSALSA software package, a tool which was first used by [Hassall et al. \(2013\)](#).

The folding algorithm works as follows. For both drift modes, the P_3 cycle is resolved in $2P_3/P$ bins. This oversampling by a factor of two implies that subsequent bins are dependent, but this gives a smoother visual result. The effective resolution was made to match the intrinsic resolution by smoothing the data using a Gaussian smoothing kernel during the folding process. Before being folded, the mode-

separated data was split in blocks of $3P_3$ pulses. Care was taken to only use blocks containing continuous stretches of pulses in a given mode, similar to what was done for the fluctuation analysis described in Sect. 3.2. Each block was first folded at a fixed value of P_3 , taken to be the average value for the given drift mode as determined from the fluctuation analysis described in Sect. 3.1. A larger block size will increase the signal-to-noise ratio per block, allowing the variability in P_3 to be better determined via the cross-correlation explained below. However, at the same time, a larger block size would cause smearing since the fixed period folding within the block might no longer be accurate enough. The variations in P_3 were taken into account by cross-correlating the folded data for each block, resulting in phase offsets, which are applied to align the average drift bands obtained for the separate blocks. This is done in an iterative manner. In the first iteration, the first block of individual pulses is used as the template in the process of cross-correlation when aligning the other blocks. In the next iteration, the over the full data set averaged modulation cycle from the previous iteration is used as the template, thus

giving a better alignment. The number of iterations was chosen such that further iterations do not lead to significant improvement in the final result.

The calculated offsets from the cross-correlation can be strongly influenced by the presence of randomly occurring bright pulses weakening the correlation of the underlying drifting subpulses pattern. For example, [Karuppusamy et al. \(2011\)](#) showed that for PSR B0031–07 the emission is a combination of drifting subpulses, nulls and sporadic bright pulses. In order to minimise the mis-alignment because of sporadic bright non-periodic emission, all samples above a certain selected threshold of intensity were clipped before folding. This means that their intensity was set to the threshold intensity when exceeding the threshold, thereby maximising the power in the drifting subpulses. This process is similar to that applied to Fig. 1 to highlight the drifting subpulses better. The offsets determined from the clipped data were used to fold the original not clipped pulse-stack. The data corresponding to the four Stokes parameters were folded identically using the offsets determined from the Stokes I pulse-stack, in which the drifting subpulses are clearest. After folding, parameters such as L , PA and χ can be determined as usual.

The P_3 -folds in Stokes I , L/I , PA, V/I and χ for both drift modes are shown in Fig. 6. The average drift bands are shown twice, above each other, in the individual panels for the purpose of continuity. Looking at the Stokes I P_3 -folds, shown in the top row of P_3 -folds in Fig. 6, clear diagonal drift bands can be seen, once more indicating that the mode separation was done correctly. The mode A drift bands (left) appear to be mostly straight diagonal bands with an intensity which is more concentrated to the central region of the profile compared to the mode B drift bands (right).

In the PA P_3 -folds (fourth row of panels from the top in Fig. 6) OPM_A (red in the online version) and OPM_B (blue in the online version) appear at different phases of the modulation cycle. This implies that throughout the modulation cycle, for both drift modes, the dominance of the two OPMs switches periodically. For drift mode A (left) it can be seen that between pulse longitudes 170° and 182° , OPM_A roughly coincides with the location of the total intensity drift band (represented by the contours), and OPM_B occurs mostly in between the total intensity drift bands. After pulse longitude 182° , an inversion occurs in the polarization such that the total intensity drift band is dominated by OPM_B , while OPM_A occurs in between the total intensity drift bands. At all pulse longitudes where in the PA distribution (Fig. 4) the dominance of OPMs alternates, the transitions are part of the modulation cycle. Also the drift mode B data (right hand side of Fig. 6) show periodic switches between the two OPMs after pulse longitude 177° , although here the total intensity drift bands are dominated by OPM_A rather than OPM_B . At earlier longitudes, OPM_B dominates at all times (see also the PA distribution in Fig. 4), hence no vertical structure is seen in the P_3 -fold.

In the P_3 -fold of L/I for drift mode A, shown below the Stokes I P_3 -fold in Fig. 6, it can be seen that the fractional linear polarization drops where the PA switching occurs (compare with the second but last left panel). Depolarization is expected to occur where OPMs mix. A similar behaviour can be seen in the L/I P_3 -fold of drift mode B for that part of the profile where OPM switching is observed.

In the P_3 -folds in V/I , displayed in the second to last row of panels in Fig. 6, it can be seen that the circular polarization is weakly modulated by the periodicity of drifting subpulses. Given that OPM_A is elliptical, we expect Stokes V to be modulated as well. Indeed we see that for mode A (left hand side), between pulse longitudes 170° and 182° , periodic switches occur between a significant circular polarization component (coinciding with OPM_A) and almost no circular polarization (coinciding with OPM_B). A similar trend can be seen for mode B after pulse longitude 170° .

In the bottom left panel, where the P_3 -fold of χ of drift mode A is shown, one can see that OPM_A has significant ellipticity, while OPM_B is almost not elliptical. Particularly interesting is an asymmetry in time (pulse number) in the ellipticity for especially drift mode A. For that mode, between pulse longitude 170° and 180° , the drift band corresponding to OPM_A starts with a lower ellipticity and it becomes highly elliptical when the OPM flips and the fractional linear polarization drops, as indicated by the (in the online version) red edge corresponding to the upper side of OPM_A in the bottom-left panel of Fig. 6. For the same drift mode, between pulse longitudes 184° and 194° , OPM_A starts highly elliptical and becomes more linear during the modulation cycle. An asymmetry is also present for drift mode B (bottom right panel), however the effect is less pronounced as for mode A. Up to pulse longitude 185° , the ellipticity of the OPM_A drift band is symmetrical in pulse number, and is maximum when the OPMs flip (bright red edge in the online version), however after this longitude only the start of the OPM_A band has a hint of ellipticity. For both drift modes, asymmetries in pulse number are only apparent in ellipticity.

4 DISCUSSION

We have discovered that for PSR B0031–07 the switches between the two OPMs are modulated synchronously with the drifting subpulses for both the A and B drift modes. This phenomenon has only been seen for four other pulsars so far, and none of those pulsars have multiple stable drift modes.

[Rankin & Ramachandran \(2003\)](#) suggested that this behaviour can be accommodated in the carousel model. In this model, drifting subpulses reflect a pattern of sub-beams circulating around the magnetic pole and the origin of this pattern is “sparking” (pair production) near the surface of the star. To explain the observed behaviour two patterns, or “images” are required, each corresponding to one of the OPMs. These two images are thought to naturally arise because of birefringence in the pulsar magnetosphere. Although at the emission height, the height where the two OPMs are produced, the ray paths corresponding to the two OPMs are identical, birefringence will cause the rays to escape the magnetosphere in different directions. As a consequence, the observed beam patterns corresponding to the OPMs differ, and provide separate distorted views (“images”) of the same underlying pattern of sparks. To explain their observations, [Rankin & Ramachandran \(2003\)](#) found that these images should be shifted both radially and azimuthally with respect to each other. Thus for PSR B0031–07, this “double imaging” should happen for (at least) both the A and B modes of

drifting, although we will point out that this picture must be more complicated for this pulsar.

Smits et al. (2005, 2007) constructed a geometrical model in order to explain the drifting subpulses (as observed in total intensity) of PSR B0031–07. The authors suggested that the emission of this pulsar comes from a carousel configuration which expands or contracts depending on the drift mode. The widest carousel configuration would correspond to drift mode A. This model can explain the fact that the intensity and occurrence of mode B drift bands decreases with increasing observing frequency, while the occurrence of mode A increases with observing frequency. This model relies on radius-to-frequency mapping (RFM; Cordes 1978), which is the effect where higher frequency emission originates from closer to the stellar surface, from magnetic field lines which are further away from the magnetic axis.

The Smits et al. (2005, 2007) model was not designed to explain the polarization properties of this pulsar. In the context of a symmetrical circular carousel, such as was applicable to PSR B0809+74 at 328 MHz (Rankin et al. 2006), one would expect to observe a symmetry of the drift bands with respect to the centre of the profile. We do not see such symmetry in the P_3 -folds of PSR B0031–07, as an inversion occurs in the PA of drift mode A (see Sect. 3.4) such that the drift band as seen in total intensity is dominated by OPM_A in one half of the profile, and OPM_B in the other half. For mode B, in the earlier part of the pulse there is only OPM_B, while in the trailing half of the profile we see switches of the OPM synchronised with the drifting subpulses. This asymmetry prevents the methodology of Rankin & Ramachandran (2003) to be applied to construct a polarized beam map for PSR B0031–07. However, it is clear that two offset images of the same carousel are not enough to explain our observations, and additional effects must play a role. These could potentially be asymmetric propagation effects in the pulsar magnetosphere. The same conclusion would apply for PSR B0818–13, which has complicated, and asymmetric, structures in its polarization, which are synchronously modulated with the drifting subpulses. Although Edwards (2004) does not discuss the asymmetry of the drift bands specifically, it was concluded that for PSR B0818–13, which has two non-orthogonal highly elliptical OPMs, a model with two offset OPM images of the same carousel is not enough to explain the observed polarization behaviour.

The fact that the P_3 -folds significantly differ for the two drift modes as observed in polarization suggests that more is happening as a simple expansion or contracting of a single carousel. Again, this could point to propagation effects to play a role, since for a changing carousel configuration the emission would propagate through different parts of the magnetosphere giving rise to different propagation effects for the different drift modes.

In the case of PSRs B0320+39 and B0818–13 (Edwards 2004), and also PSR B0809+74 at both 328 MHz and 1380 MHz (Edwards 2004; Rankin et al. 2006), the total intensity drift bands are dominated by one OPM, while the other OPM dominates in between drift bands. PSR B0031–07 is different, since the total intensity drift band in drift mode A is dominated by different OPMs in the leading and trailing half of the profile. Looking at the P_3 -fold of drift mode A in PA (fourth row of panels from the top in Fig. 6), the pattern traced by a given OPM appears

to be split in the middle of the profile with a vertical offset appearing. This at least visually resembles a subpulse phase jump as seen, for example, in the total intensity drift bands of PSR B0320+39 (Edwards et al. 2003). For PSR B0031–07 the total intensity P_3 folds are more continuous, although coincident with the discontinuity as seen in the PA P_3 -fold of drift mode A, a small change in the slope of the intensity drift band can be seen, such that the drift band becomes shallower after the discontinuity. Edwards et al. (2003) suggested that a subpulse phase jump is another type of phenomenon which might require superposed images of the same carousel system. Here each image should have drifting subpulses which are out of phase because of an azimuthal offset. To explain the subpulse phase jump, each image should dominate in different halves of the profile. At the longitude where the phase modulation jump occurs, in the middle of the profile, the two images destructively interfere. Edwards (2004) pointed out that if the two superposed out of phase images correspond to the two OPMs, both the subpulse phase step as seen in total intensity and the synchronous switching of the dominant OPM can be explained. Edwards & Stappers (2003) observed the intensity phase modulation of PSR B0320+39 at 328 and 1380 MHz and noted that the change in the phase jump with frequency could be explained if the centre of the carousel systems are offset from each other. So there would be a precedent to explore if a model which is more complicated than just a shrinking or expanding carousel would apply to PSR B0031–07 as well.

Other authors (e.g. Clemens & Rosen 2004, 2008; Rosen & Demorest 2011) suggested that non-radial oscillations of the surface of the neutron star could explain drifting subpulses as well as the subpulse phase steps observed in total intensity drift bands. However, it is unclear in this model how the polarization is expected to be affected, and why for PSR B0031–07 no subpulse phase step would be observed in total intensity, while there is a discontinuity in the PA of the drift bands in the middle of the profile.

It is intriguing that the ellipticity evolves asymmetrically throughout the modulation cycle (in pulse number), such that in drift mode A in the leading half of the profile, the emission becomes elliptical just before the emission flips from OPM_A (which as found in Sect. 3.3 is significantly more elliptical on average) to OPM_B, but not when OPM_B flips to OPM_A. Hence, the ellipticity of the OPMs are not fixed during the modulation cycle. In the carousel model, the pattern of circulating sub-beams is in general taken to be symmetric with respect to the sense of circulation, in the sense that the structure of the sub-beam is similar in its leading and trailing half. Here, some form of symmetry breaking is required by physics which is affected by the sense of the circulation. Similar symmetry breaking has not been seen for the other four pulsars which show OPM switches synchronous with drifting subpulses. The origin of this asymmetry is unclear, but coherent interference by the two OPMs could play a role.

From theory (e.g. Arons & Barnard 1986) one could expect the OPMs to be purely linearly polarized. However, this is not the case for PSR B0031–07. Also PSR B0329+54 has two OPMs with different degrees of ellipticity (Edwards & Stappers 2004). The authors explained this in terms of Generalised Faraday Rotation (GFR, Kennett & Melrose 1998) and coherent addition of the radiation of the two OPMs, which allows partial conversion of linear into circular po-

larization. GFR would contribute to frequency dependent polarization effects as well (see [Ilie et al. \(2019\)](#) and references therein). [Melrose et al. \(2006\)](#) offered an alternative explanation for the observed variable polarization properties of individual pulses of PSR B0329+54, by assuming incoherent addition of the radiation of the two OPMs. In general it is hard to distinguish whether the observed polarized radiation is the incoherent or coherent sum of OPMs. For PSR B0031–07, when the rate of occurrence of both OPMs is comparable in the PA distribution of the not drift-mode separated dataset, the linear polarization is generally low, while when the rate of occurrence of one OPM is higher, as seen for the drift mode A separated dataset, L is also higher. This is compatible with a scenario where the observed radiation is an incoherent sum of OPMs. On the other hand, as pointed out for example by [Dyks \(2017\)](#), a good indicator for the natural polarization modes being coherently combined would be the presence of a peak of circular polarization near an OPM transition, while L/I decreases and the total polarization is not affected. Fig. 4 shows that the ellipticity angle peaks where the OPM transitions occur for drift mode A (longitudes 171° and 178°), however the average total polarization does significantly drop. So it seems likely there is a combination of coherent and incoherent OPM summation (partial coherent addition) occurring in PSR B0031–07.

5 SUMMARY AND CONCLUSIONS

We established, using the P_3 -folding technique, that for PSR B0031–07 the orthogonal polarization modes switch synchronously with the drifting subpulses seen in total intensity. This is observed for both drift modes (out of a total of three) which are present at our observing frequency ([Smits et al. 2005, 2007](#)). A similar connection between the periodicity seen in polarization and total intensity has only been reported for four other pulsars ([Ramachandran et al. 2002](#); [Rankin & Ramachandran 2003](#); [Edwards 2004](#)). PSR B0031–07 is the only pulsar in this group of pulsars which shows drift mode changes, making it a unique source to test emission models.

PSR B0031–07 is also different from the other four pulsars, as it was found that the ellipticity evolves asymmetrically with time during the modulation cycle, such that the ellipticity is high just before the emission flips from one OPM to the other, but not when it flips back. The asymmetry is different for the two drift modes. In the carousel model, some form of symmetry breaking would be required by physics which is affected by the sense of the circulation, which is likely related to coherent mode addition effects.

For all other four pulsars which show modulated OPM switches synchronous with drifting subpulses, the drift bands observed in total intensity are generally dominated by one OPM, while the other one dominates in between the drift bands. However, during drift mode A of PSR B0031–07, the drift bands as observed in total intensity are dominated by different OPMs in different halves of the profile. This is accompanied by a slight change of the slope of the intensity drift band in the middle of the profile. This could be related to what is known as subpulse phase steps ([Edwards et al. 2003](#)) and could hint towards two superposed out of phase images of the carousel. The production of two images is also

a requirement to explain the observed periodic changes in polarization.

It will be challenging to construct a geometric model for the polarized properties of the drifting subpulses of PSR B0031–07. A symmetrical carousel which contracts or expands when switching between drift modes, as was suggested by [Smits et al. \(2005, 2007\)](#) for PSR B0031–07, can only explain the behaviour as seen in total intensity. Additional effects would be required in order to explain the here presented polarization observations which show large asymmetries between the leading and trailing halves of the profile. This is likely to be because of propagation effects in the pulsar magnetosphere, including birefringence which can cause the emission produced by the carousel to be spatially split in two distinct images corresponding to two OPMs. In addition, it is suggested that a combination of coherent and incoherent mode addition plays a role in forming the observed polarization state of the radiation. To explain the large asymmetries as seen in the leading and trailing half of the profile, especially the P_3 -fold as observed in PA, we speculate that more complex propagation effects play a role, such as the coupling between the two OPMs during the propagation through the magnetosphere. If this coupling is asymmetric as function of pulse longitude, one could expect asymmetries to be observed, while maintaining the picture of a symmetric underlying carousel configuration.

ACKNOWLEDGEMENTS

The authors would like to thank Ben Shaw for providing the ephemeris used in the folding process. In addition we would like to thank Crispin Agar and Geoff Wright for the many useful discussions related to the interpretation of the results in this manuscript. The Parkes radio telescope is part of the Australia Telescope which is funded by the Commonwealth of Australia for operation as a National Facility managed by CSIRO. Pulsar research at Jodrell Bank Centre for Astrophysics and Jodrell Bank Observatory is supported by a consolidated grant from the UK Science and Technology Facilities Council (STFC).

REFERENCES

- Allen M. C., Melrose D. B., 1982, *Proceedings of the Astronomical Society of Australia*, 4, 365
- Arons J., Barnard J. J., 1986, *ApJ*, 302, 120
- Backer D. C., 1970, *Nature*, 227, 692
- Backer D. C., Rankin J. M., Campbell D. B., 1976, *Nature*, 263, 202
- Basu R., Mitra D., Melikidze G. I., Maciesiak K., Skrzypczak A., Szary A., 2016, *ApJ*, 833, 29
- Basu R., Mitra D., Melikidze G. I., Skrzypczak A., 2019, *MNRAS*, 482, 3757
- Chen T., 2015, Master’s thesis, The University of Manchester
- Clemens J. C., Rosen R., 2004, *ApJ*, 609, 340
- Clemens J. C., Rosen R., 2008, *ApJ*, 680, 664
- Cordes J. M., 1978, *ApJ*, 222, 1006
- Deshpande A. A., Rankin J. M., 1999, *ApJ*, 524, 1008
- Deshpande A. A., Rankin J. M., 2001, *MNRAS*, 322, 438
- Drake F. D., Craft H. D., 1968, *Nature*, 220, 231
- Dyks J., 2017, *MNRAS*, 472, 4598
- Edwards R. T., 2004, *A&A*, 426, 677

- Edwards R. T., Stappers B. W., 2002, *A&A*, **393**, 733
- Edwards R. T., Stappers B. W., 2003, *A&A*, **410**, 961
- Edwards R. T., Stappers B. W., 2004, *A&A*, **421**, 681
- Edwards R. T., Stappers B. W., van Leeuwen A. G. J., 2003, *A&A*, **402**, 321
- Fung P. K., Khechinashvili D., Kuijpers J., 2006, *A&A*, **445**, 779
- Gangadhara R. T., 1997, *A&A*, **327**, 155
- Gil J. A., Sendyk M., 2003, *ApJ*, **585**, 453
- Gogoberidze G., Machabeli G. Z., Melrose D. B., Luo Q., 2005, *MNRAS*, **360**, 669
- Hassall T. E., et al., 2013, *A&A*, **552**, A61
- Hewish A., Bell S. J., Pilkington J. D. H., Scott P. F., Collins R. A., 1968, *Nature*, **217**, 709
- Huguenin G. R., Taylor J. H., Troland T. H., 1970, *ApJ*, **162**, 727
- Ilie C.-D., Weltevrede P., 2018, in Weltevrede P., Perera B. B. P., Preston L. L., Sanidas S., eds, IAU Symposium Vol. 337, Pulsar Astrophysics the Next Fifty Years. pp 79–82, doi:10.1017/S1743921317009991
- Ilie C. D., Johnston S., Weltevrede P., 2019, *MNRAS*, **483**, 2778
- Johnston S., Kerr M., 2018, *MNRAS*, **474**, 4629
- Karuppusamy R., Stappers B. W., Serylak M., 2011, *A&A*, **525**, A55
- Kennett M., Melrose D., 1998, *Publ. Astron. Soc. Australia*, **15**, 211
- Komesaroff M. M., 1970, *Nature*, **225**, 612
- Lyubarsky Y. E., 2002, in Becker W., Lesch H., Trümper J., eds, Neutron Stars, Pulsars, and Supernova Remnants. p. 230 (arXiv:astro-ph/0208566)
- Manchester R. N., 1975, *Proceedings of the Astronomical Society of Australia*, **2**, 334
- Manchester R. N., Taylor J. H., Huguenin G. R., 1975, *ApJ*, **196**, 83
- McSweeney S. J., Bhat N. D. R., Tremblay S. E., Deshpande A. A., Ord S. M., 2017, *ApJ*, **836**, 224
- Melrose D. B., 1979, *Australian Journal of Physics*, **32**, 61
- Melrose D., Miller A., Karastergiou A., Luo Q., 2006, *MNRAS*, **365**, 638
- Petrova S. A., 2001, *A&A*, **378**, 883
- Petrova S. A., Lyubarskii Y. E., 2000, *A&A*, **355**, 1168
- Radhakrishnan V., Cooke D. J., 1969, *Astrophys. Lett.*, **3**, 225
- Ramachandran R., Rankin J. M., Stappers B. W., Kouwenhoven M. L. A., van Leeuwen A. G. J., 2002, *A&A*, **381**, 993
- Rankin J. M., Ramachandran R., 2003, *ApJ*, **590**, 411
- Rankin J. M., Ramachandran R., van Leeuwen J., Suleymanova S. A., 2006, *A&A*, **455**, 215
- Rosen R., Demorest P., 2011, *ApJ*, **728**, 156
- Ruderman M. A., Sutherland P. G., 1975, *ApJ*, **196**, 51
- Smits J. M., Mitra D., Kuijpers J., 2005, *A&A*, **440**, 683
- Smits J. M., Mitra D., Stappers B. W., Kuijpers J., Weltevrede P., Jessner A., Gupta Y., 2007, *A&A*, **465**, 575
- Taylor J. H., Huguenin G. R., Hirsch R. M., Manchester R. N., 1971, *Astrophys. Lett.*, **9**, 205
- Vivekanand M., Joshi B. C., 1997, *ApJ*, **477**, 431
- Weltevrede P., 2016, *A&A*, **590**, A109
- Weltevrede P., Johnston S., 2008, *MNRAS*, **391**, 1210
- Weltevrede P., Stappers B. W., van den Horn L. J., Edwards R. T., 2003, *A&A*, **412**, 473
- Weltevrede P., Edwards R. T., Stappers B. W., 2006, *A&A*, **445**, 243
- Weltevrede P., Stappers B. W., Edwards R. T., 2007, *A&A*, **469**, 607
- Wright G. A. E., 2003, *MNRAS*, **344**, 1041
- Wright G. A. E., Fowler L. A., 1981, in Sieber W., Wielebinski R., eds, IAU Symposium Vol. 95, Pulsars: 13 Years of Research on Neutron Stars. p. 211
- van Leeuwen J., Timokhin A. N., 2012, *ApJ*, **752**, 155
- van Leeuwen A. G. J., Kouwenhoven M. L. A., Ramachandran R., Rankin J. M., Stappers B. W., 2002, *A&A*, **387**, 169
- van Straten W., Bailes M., 2011, *Publ. Astron. Soc. Australia*, **28**, 1

This paper has been typeset from a T_EX/L^AT_EX file prepared by the author.